Journal of Materials Science: Materials in Electronics (2018) 29:4869–4880
https://doi.org/10.1007/s10854-017-8444-7

Reduced graphene oxide (rGO): supported NiO, Co_3O_4 and $NiCo_2O_4$ hybrid composite on carbon cloth (CC)—bi-functional electrode/catalyst for energy storage and conversion devices

R. Tamilselvi[1] · N. Padmanathan[2] · K. Mani Rahulan[3] · P. Mohana Priya[4] · R. Sasikumar[5] · M. Mandhakini[1]

Received: 12 August 2017 / Accepted: 18 December 2017 / Published online: 26 December 2017

Abstract
In the present work, we have synthesized a series of composites with NiO, Co_3O_4, and $NiCo_2O_4$ and reduced graphene oxide (RGO). The hybrid composites were fabricated trough a single step hydrothermal approach with subsequent heat treatment. X-ray diffraction, Raman spectroscopy and Transmission Electron Microscopy analyses indicate the metal oxide nanoparticles were integrated well in the carbon cloth substrate with rGO support. The as-prepared materials were evaluated as the electrodes for energy storage and conversion devices. As the electrode for supercapatteries, rGO supported $NiCo_2O_4$ exhibits highest specific capacity of 333 C g^{-1} at a specific current of 1 mA cm^{-1} when compared to their monometallic oxides and also exhibits excellent cycling stability with 89% retention at 5 mA cm^{-1} after 5000 cycles in a three-electrode system. Furthermore, we have investigated the electro-oxidation of methanol with these electrode in an alkaline medium. Compared to individual oxide composites, the $NiCo_2O_4$–rGO electrode shows excellent electro-catalytic activity towards methanol oxidation with low onset potential of ~0.3 V and high catalytic current density. The observed bi-functionality of rGO supported metal oxide composite could be attributed to the enhanced electrical conductivity and the well-integrated contact with carbon cloth back bone. Thereby it can be concluded that the design of hybrid composite electrode could be the better choice of electro-active materials for both energy storage and conversion applications.

1 Introduction

The demand for clean and sustainable energy has been continuously increasing due to the exhaustion of conventional fossil fuels and their linked ecological issues [1]. These consequences makes it necessary to focus intensive research towards the development of advanced energy storage and conversion devices. Recently, supercapacitors (SCs) and direct methanol fuel cells (DMFCs) have received great research interest as high performance energy storage and conversion devices [1–10]. Both of these devices require promising electroactive materials with featured electrochemical activity (i.e., multiple oxidation states, low onset potential, more surface active sites for redox reaction etc. that affect the exchange current density) [2, 5, 7, 10]. Till date, the practical requirement of electrochemical devices have not been achieved with the single element or compound electrodes. However, there is a possibility to achieve the desirable device performance with the hybrid and composite materials that combine the unique characteristics of each component to surpass the limitations of the single materials [11]. Therefore, it is essential to discover novel

Electronic supplementary material The online version of this article (https://doi.org/10.1007/s10854-017-8444-7) contains supplementary material, which is available to authorized users.

✉ N. Padmanathan
padmanmsc@gmail.com

✉ M. Mandhakini
mandhakini7@gmail.com

[1] Center for Nanoscience and Technology, Anna University, Chennai 600 025, India

[2] Tyndall National Institute, University College Cork, Cork, Ireland

[3] Department of Physics and Nanotechnology, SRM University, Chennai 600 102, India

[4] Department of Physics, Indian Institute of Technology Tirupati, Tirupati 600 032, India

[5] Department of Chemical Engineering, Anna University, Chennai 600 025, India

and environmentally friendly multifunctional hybrid electrode materials for both energy storage and conversion applications.

In a related process, the performance of DMFCs is directly related to the catalyst activity used to oxidize the liquid fuel. In this view, transition metal oxides (TMOs), hydroxides, and their compounds are being extensively demonstrated for high capacity supercapacitors with enhanced energy density and non-precious catalyst for DMFCs because of their more abundance in nature, less toxicity, and tuneable microstructures [12–20]. These materials provide with high surface area, good structural stability, electrical conductivity and processability and can shows enhanced electro-catalytic activity relevant to both of these energy storage and conversion technologies [21–24]. However, these electrodes limit their further practical applications due to inadequate conductivity to support rapid electrode kinetics during redox process [25]. In order to increase the intrinsic electrical conductivity of the electrode, the conductive carbon materials are being proposed as a backbone support [25, 26]. Most efforts have been focused to synthesis composite electrode with activated carbon (AC), carbon nanotubes (CNTs) and reduced graphene oxide (rGO) [27]. However, the electrode performance is still not satisfactory due to the dissolution and detachment of the metal oxide from the carbon support. Hence the recent studies focuses the direct integration of metal oxide nanostructure onto conductive substrate. In particular the flexible carbon cloth (CC) have received more attention owing to its unique functional features including large surface area, high porosity, good electric conductivity, and excellent chemical stability in a wide variety of liquid electrolytes [25]. Although, CC supported electrode materials have been extensively studied for batteries, supercapacitors and fuel cells [28–32], many approaches have been explored, in particular graphene-based nanocomposites for the fabrication of high-performance supercapacitors and fuel cells [33]. However composite of rGO supported hybrid metal oxides nanostructures grown on carbon cloth is rarely been reported. The inherent properties of rGO and CC such as high surface area, electrical conductivity, high porosity and high stability related to the specific capacitance will increase the electrode performance and the catalytic properties.

The second important property is the long term resistance from corrosion in alkaline medium, and in this regard nickel–cobalt–rGO hybrid materials are found to be attractive as the superior electrode/catalyst for electrochemical energy storage and conversion. Dong et al. reported 3D graphene supported Co_3O_4 nanowires for high performance supercapacitor [34]. Recently, Ni–Co binary oxide/reduced graphene oxide composite has been reported for supercapacitor by Bai et al. [35]. Similarly, Gao et al. reported the improved electrochemical performance with rGO/NiO composite electrode towards supercapacitor application [36]. Equally, these materials are being utilized as the catalyst for DMFCs, recently, Yu et al. investigated $NiCo_2O_4$ anchored on 3D graphene for methanol oxidation [37]. In continuation, Hassen et al. demonstrated $Co(OH)_2$/graphene mesostructures as the ethanol oxidation catalyst [38] followed by graphene/NiO nanocomposite as efficient electro-catalyst for methanol oxidation by Li et al. [39]. However the simultaneous growth of rGO/metal oxide using cost-effective synthesis process is limited and needs to be explored.

In the present study, we developed a novel synthetic strategy to fabricate bifunctional rGO supported hybrid metal oxides (MOs) nanostructure on carbon cloth substrate and investigated for both energy storage and conversion applications. One-pot hydrothermal approach has been followed to design rGO/MOs (M = Ni and Co) on CC substrate. The electrochemical characteristics of as fabricated hybrid nanostructures has been examined as a high performance flexible non-capacitive faradaic energy storage electrode and electro-catalyst for methanol oxidation. Among the prepared materials, the bimetallic rGO/$NiCo_2O_4$ hybrid electrode has delivered a maximum specific capacity of 333.3 C g^{-1} at a constant current of 1 mA cm^{-2} and a long-term stability for supercapatteries. In addition, the electrode showed superior electrocatalytic activity with lower onset potential (0.31 V) and greater stability for methanol oxidation. This bifunctional activity is principally due to the integrative consequence of both Ni and Co active sites with graphene intercalation in addition to the well supported CC. These results further open-up a new platform for large scale production and utilization of hybrid electrodes based on transition metal oxides and graphene for energy storage and conversion devices.

2 Experimental procedure

2.1 Fabrication of hybrid composites

The synthesis of hybrid electrode involved two steps, preparation of Graphite oxide followed by simultaneous growth of metal oxides/rGO on carbon cloth using hydrothermal approach. The precursors and solvents were all analytical grade and used as received without further purification. The graphite oxidation was done by well-known modified Hummer's method. In detail, 1 g of graphite flakes and 0.5 g of $NaNO_3$ were mixed with 30 mL of concentrated H_2SO_4 in ice bath (0–5 °C) under constant stirring. Subsequently, 8 g of $KMnO_4$ was slowly added to the graphite mixture and continued stirring for 30 min. Then 100 mL of DI water was added dropwise into the above oxidized graphite in order to quench the reaction. Brownish yellow mixture was obtained and the stirring was further continued at 30 °C for 4 h.

Followed by addition of 20 mL of H_2O_2 (28%) was added to the solution. The end product was repeatedly washed with diluted HCl solution followed by DI water until to reach the neutral pH. Finally, Graphite oxide suspension was dried under vaccum at 60 °C for overnight and used for further hydrothermal reduction process with metal oxides.

To design the rGO/metal oxide hybrid electrode, the flexible substrate carbon cloth (CC) was pre-treated with 3 M HCl through ultra-sonication followed by washing with deionized (DI) water. The hydrothermal growth process was same as that of our previous report [30]: typically, 1 mg/mL of GO was ultrasonically (1 h) dispersed in equal volume of mixed solvent ethanol/water (40/40 mL) which contains pre-treated CC (4 cm × 4 cm), 0.01 M of $Ni(NO_3)_3{\cdot}6H_2O$, 0.02 M of $Co(NO_3)_3{\cdot}6H_2O$ and excess amount of urea (0.1 M) for CC@rGO/$NiCo_2O_4$ hybrid material. Whereas for CC@rGO/NiO and CC@rGO/Co_3O_4 only 0.01 M of $Ni(NO_3)_3{\cdot}6H_2O$ and 0.01 M $Co(NO_3)_3{\cdot}6H_2O$ respectively were alone dissolved. The other procedure is followed same as before. After that, the homogenous solution was transferred to a stainless steel autoclave and kept at 180 °C for 12 h in an oven. Finally, the oven was cooled down to room temperature naturally and CC was separated out from the container and washed with DI water thrice. Then it is allowed to undergo heat treatment in muffle furnace at 300 °C for 3 h in air. To make easy identification the materials were labelled as CCG, CC@NG, CC@CG and CC@NCG in respective of pristine rGO, rGO/NiO@CC, rGO/Co_3O_4@CC and rGO/$NiCo_2O_4$@CC. The mass loading of the composite was measured carefully from the weight difference of the substrates before and after the hydrothermal growth of materials. The estimated approximate mass loading of the composites were ~ 0.5, ~ 0.9, ~ 1.2 and 1 mg cm^{-2} for CCG, CC@NG, CC@CG and CC@NCG respectively.

3 Materials characterization

The phase of CC-supported hybrid electrodes were characterized using X-ray diffractometer (XRD) (Bruker D2-PHASER). Raman spectra of the samples were taken under visible excitation at 514.3 nm using a Laser Raman Spectrophotometer. The morphologies of all the samples were observed under a (FEI 200F HRSEM) scanning electron microscopy after sputtering the samples with platinum for 30 s. Energy dispersive X-ray measurements were conducted using the EDAX system attached to the same microscope. High resolution transmission electron microscope was carried out in TECNAI HRTEM-3010 at 200 kV. Electrochemical characterization was carried out at room temperature using CHI 7007C electrochemical workstation. The fabricated hybrid electrodes were used as the binder-free working electrode. A three electrode cell was constructed with the working electrode, Pt wire counter electrode and saturated calomel electrode (SCE) as a reference electrode. The 3 M KOH aqueous solution was used as the supporting electrolyte. Similarly, for fuel cell application, the electrocatalytic-activity of the electrode was studied in 1 M KOH solution with and without 0.5 M CH_3OH by cyclic voltammetry and chronoamperometry.

4 Results and discussion

The crystal structures of the rGO incorporated NiO, Co_3O_4 and $NiCo_2O_4$ grown over carbon cloth were investigated by XRD analysis. Figure 1 shows the XRD pattern of the pure CC, CCG, CC@NG, CC@CG and CC@NCG hybrid electrodes. The observed X-ray diffractions peaks are found to be intense and broad indicating polycrystalline nature with nano-sized crystallites. In Fig. 1, the NiO peak intensity for CC@NG electrode is very low, thereby it has shown in Fig. S1 (supplementary information) as separate graph in order to support the growth of NiO. The diffraction peak positions match well with standard diffraction patterns (CC@NG #47-1049; CC@CG #78-1970; CC@NCG #20-0781) and the reflections can be indexed to the respective crystal planes as shown in Fig. 1. The pure CC showed well-known XRD peaks related to the graphite (JCPDS 08-0415) [30]. In CCG sample, the observed peak shift at 2θ value of graphite approximately 24°–26° indicating the successful formation of reduced graphene oxide on CC. Based on the metal oxide, the characteristic peaks at the corresponding 2θ values as indexed in the XRD pattern are respectively attributed to the diffraction of peaks of crystalline metal oxides. Nevertheless, the diffraction peak related to rGO is

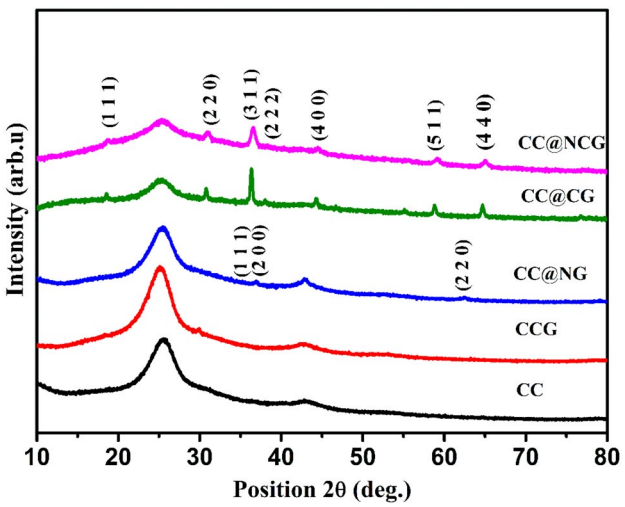

Fig. 1 XRD pattern pure carbon cloth, pristine rGO@CC, NiO@CC, Co_3O_4@CC and $NiCo_2O_4$@CC

not distinguishable in the hybrid CC@NG, CC@CG and CC@NCG due to its low content or low degree of graphitization [40]. No other secondary phase is detected, indicating a well-defined crystal structure with high quality of hybrid electrode.

In order to further confirm the growth of rGO/metal oxide hybrid materials, the Raman spectroscopy was used. Figure 2 shows the Raman spectra of the as prepared hybrid CCG, CC@NG, CC@CG and CC@NCG samples in addition to the pure CC. All the samples exhibits the D-band (arising from the edge or defect sites of carbon) and (G-band representing the sp^2 carbon) vibrations with different intensity associated to metal oxide at 1345 and 1588 cm^{-1} respectively [41]. Pristine CC and CCG showed only the disordered carbon and graphitic carbon bands. With the metal oxide, there is few more additional bands at low wavenumber which indicating that incorporation of rGO into metal oxide nanostructures. For CC@CG electrode, the Raman spectra is distinct and prominent oxide bands are observed as shown in Fig. 2. The well resolved Raman peaks at 190, 474 and 687 cm^{-1}, can be attributed to the E_g, F_{2g} and A_{1g} modes of Co_3O_4 [34, 42]. However, the carbon bands with diminished intensity in CC@CG further reveals the prominent growth of Co_3O_4 and is in consistent with XRD analysis. In the CC@NG, the characteristic Ni–O peak appeared at 508 cm^{-1}, whereas for CC@NCG, more bands are observed at 188, 471, 509, and 649 cm^{-1}, related to F_{2g}, E_g, F_{2g}, and A_{1g} modes of the $NiCo_2O_4$ nanostructure, respectively [30, 43].

The surface morphology of the rGO/metal oxide composites were examined by FE-SEM, as shown in Fig. 3a–d and Fig. S2a–h. SEM image of CCG (Fig. 3a) showed the attachment of graphene layers on carbon cloth. The coverage of rGO incorporated NiO flakes on the CC surface can be observed for CC@NG in Fig. 3b. Freestanding NiO nanoflakes are uniformly grown onto the flexible carbon fiber. From Fig. 3c, it can be seen that dense growth of Co_3O_4 nanoparticles with graphene when CC acted as flexible template as well as substrate. Additionally, the graphene/Co_3O_4 composites experienced a strong aggregation during growth when compared to other two composites. This result is well consistent with XRD and Raman analysis. $NiCo_2O_4$ nanospheres anchored on the carbon fiber can be observed in the FE-SEM image of CC@NCG as shown in Fig. 3d and Fig. S2g, h. In this case, the well distributed nanospheres are formed during hydrothermal treatment in addition to rGO. In comparison with the FESEM image of CCG, the surface of the composites are much rougher, which is attributed to the growth of the metal oxides with RGO during hydrothermal process. Further it reveals that rGO are enclosed by the aggregated metal oxides when oxide fractions are comparatively very high.

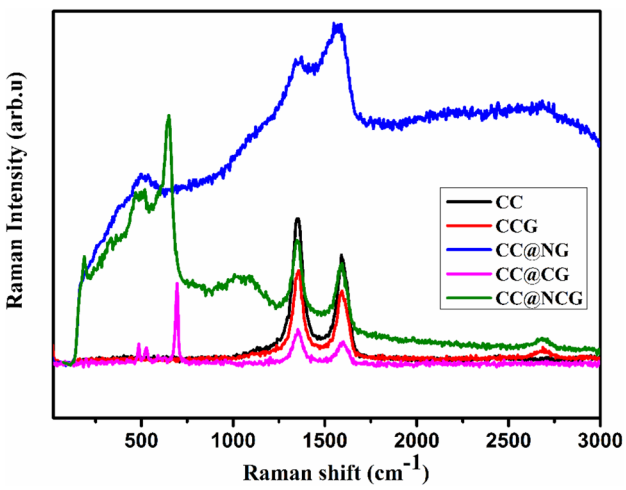

Fig. 2 Raman Spectra of pure and hybrid composite materials grown on carbon cloth

To understand the microstructure, the TEM analysis was carried out for the samples scratched off ultrasonically from the CC substrate. Figure 5a–h shows the TEM images of the hybrid composites with their corresponding SAED pattern. The Pristine CCG showed transparent reduced graphene oxide sheets with tri-layered structure. The observed diffraction pattern of CCG confirms the crystalline structure with the reflection of (1100) plane [41]. From the TEM image of CC@NG shown in Fig. 5c, it can be seen that stacked flake like NiO–rGO composite structure. The corresponding SAED pattern in Fig. 5d shows the dispersed ring patterns, indicating the polycrystalline nature of the NiO nanoflakes. However, from the TEM image of CC@CG composite as shown in Fig. 5e, it can be found that the Co_3O_4 nanoparticles are attached in the rGO sheets. Additionally, the SAED pattern of Co_3O_4/rGO composite presented in the Fig. 5f showed diffused rings which infers the high crystallinity of the CC@CG composite. The observed diffraction pattern matched well with the typical spinel crystal structure of Co_3O_4. Furthermore, the TEM image of the CC@NCG composite designate that spherical $NiCo_2O_4$ nanoparticles were homogeneously deposited on the surface of CC in addition with rGO. Also, the well-defined rings in the SAED pattern (Fig. 5h) specifies the polycrystalline characteristics of the $NiCo_2O_4$/rGO composite, and the rings could be assigned to the appropriate crystal planes of (111), (220), (311), and (400) of spinel nickel cobaltite [30]. The energy dispersive spectra analysis of the prepared metal oxide/rGO composite is shown in Fig. 4a–d. The corresponding EDS spectra shows the primary elements of Ni, Co, C, and O exhibit in the appropriate composition without any impurities.

To investigate the electrochemical behaviors of the metal oxide/rGO composite electrodes, cyclic voltammetry (CV) and galvanostatic charge–discharge (GCD) techniques were applied. All the electrochemical performances of the

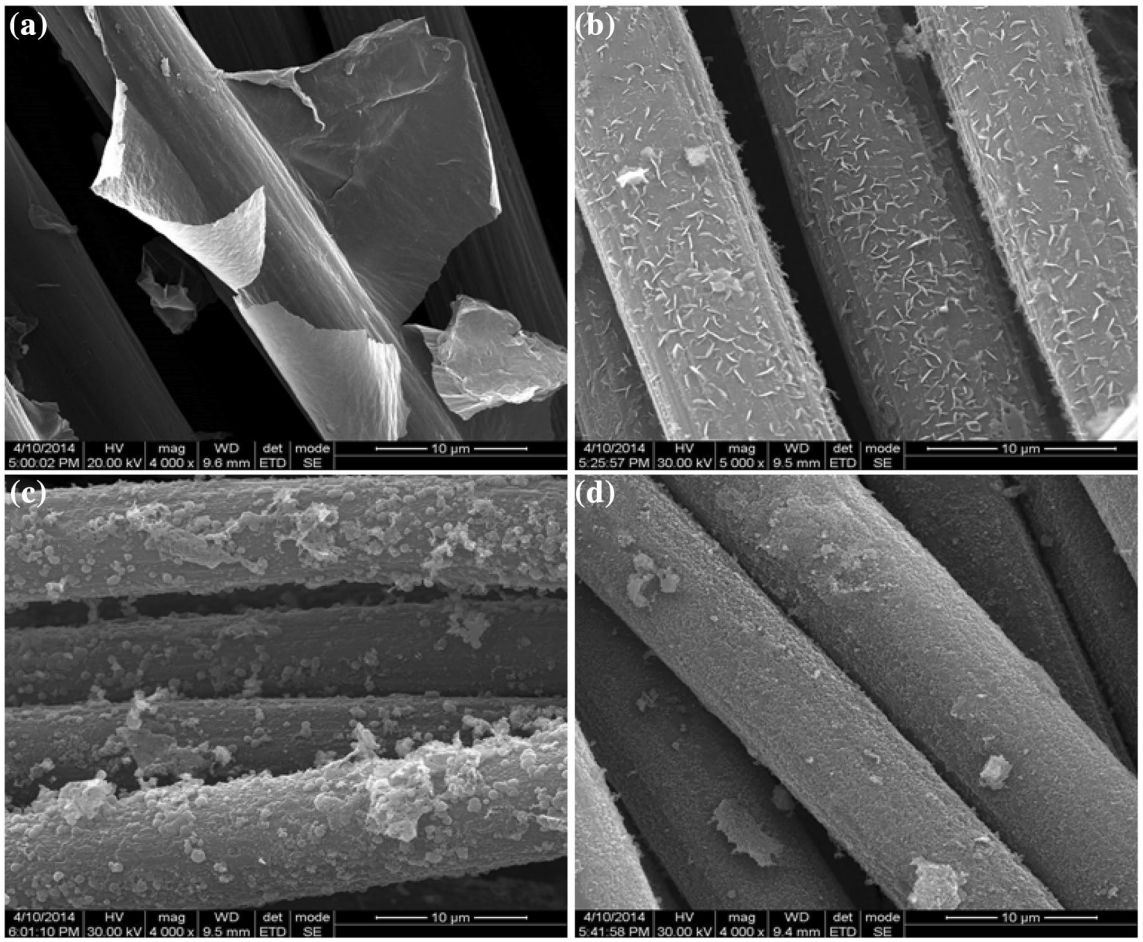

Fig. 3 HRSEM images of **a** CCG, **b** CC@NG, **c** CC@CG and **d** CC@NCG

as–prepared metal oxide/rGO composites are examined in three electrode configuration with 3 M KOH electrolyte solution and shown in Fig. 6a–d. CV is one technique used to distinguish capacitive or non-capacitive characteristic of the electrode materials. Basically, rectangular CV curves indicates the ideal electrochemical double layer capacitive nature of the electrode which has been observed in carbon based materials [44]. Noteworthy, the transition metal oxide identified with their surface redox activity and thereby named as the pseudo-capacitive electrode [45]. In general, metal oxide electrodes are used to describe by the term pseudo-capacitive. However, these electrode does not exhibit the linear relationship between potential and current like an ideal capacitor except the RuO_2 and MnO_2 [46–48]. Hence, such a non-capacitive faradaic type charge storage process should be excluded from discussions on pseudo-capacitive faradaic processes. Due to the misconception of the term pseudo-capacitance, many researchers have categorized their materials as the electrode for supercapacitor which showed battery like redox profile [46]. Figure 6a shows the CV curves of the pure and composites electrodes at a scan rate of 5 mV s^{-1}. The bare CC and CCG electrode shows the rectangular shape CV response, indicating capacitive behavior of the carbon structures. As seen in Fig. S3a, the CV current density increases gradually with the increase of the scan rate, and retains rectangular shape even at 50 mV s^{-1}. Ultimately, the rGO/metal oxide hybrid electrodes showed distinct CV curve as shown in Fig. 6a. All the composite electrode have showed pair of oxidation/reduction peak in the CV curve indicating the faradaic charge storage mechanism of the electrodes. The observed redox couples mainly due to the reversible reaction of MO/MOOH formed on the CC surface and the faraday reaction of OH^- with the residual function groups in the rGO. The redox couples are corresponding to the following faradic reactions (Eqs. 1–4):

$$NiO + OH^- \leftrightarrow NiOOH + e^- \quad (1)$$

$$Co_3O_4 + OH^- + H_2O \leftrightarrow 3CoOOH + e^- \quad (2)$$

$$NiCo_2O_4 + OH^- + H_2O \leftrightarrow NiOOH + 2CoOOH + e^- \quad (3)$$

$$CoOOH + OH^- \leftrightarrow CoO_2 + H_2O + e^- \quad (4)$$

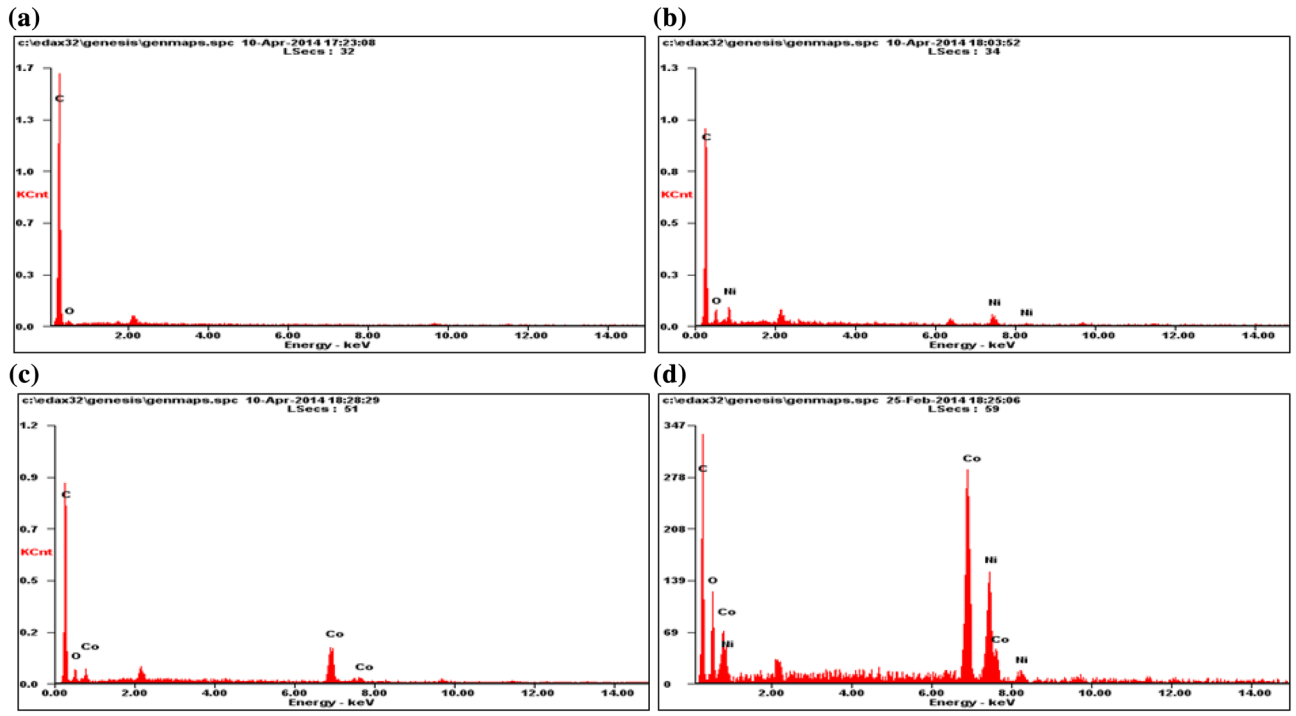

Fig. 4 EDS spectra of **a** CCG, **b** CC@NG, **c** CC@CG and **d** CC@NCG

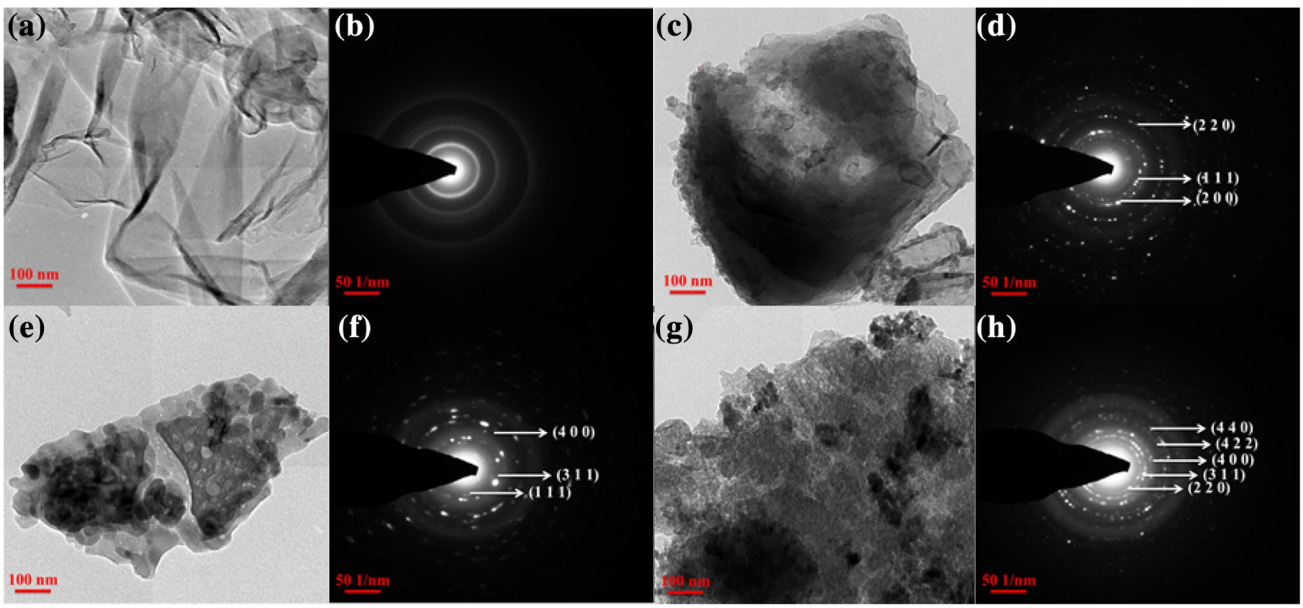

Fig. 5 HRTEM images and the corresponding SAED pattern of **a, b** CCG, **c, d** CC@NG, **e, f** CC@CG and **g, h** CC@NCG

Among them, the large area under CV of CC@NCG electrode reflects enhanced electrode conductivity due to the rGO. When compared to monometallic electrode, composite electrode CC@NCG showed well-distinct two pair of redox peaks corresponding to the reversible reaction of both $Co^{2+/3+}$ and $Ni^{2+/3+}$. It is interesting to point out that, this dual redox features is generally not discernible in bimetallic electrodes and only one redox peak of $Co^{2+/3}$ was observed based on the earlier reports. In our earlier report on $NiCo_2O_4$/CFC nanostructures also showed only one redox pair [43, 49]. Here, the two redox pair may be attributed to the strong chemical interaction between

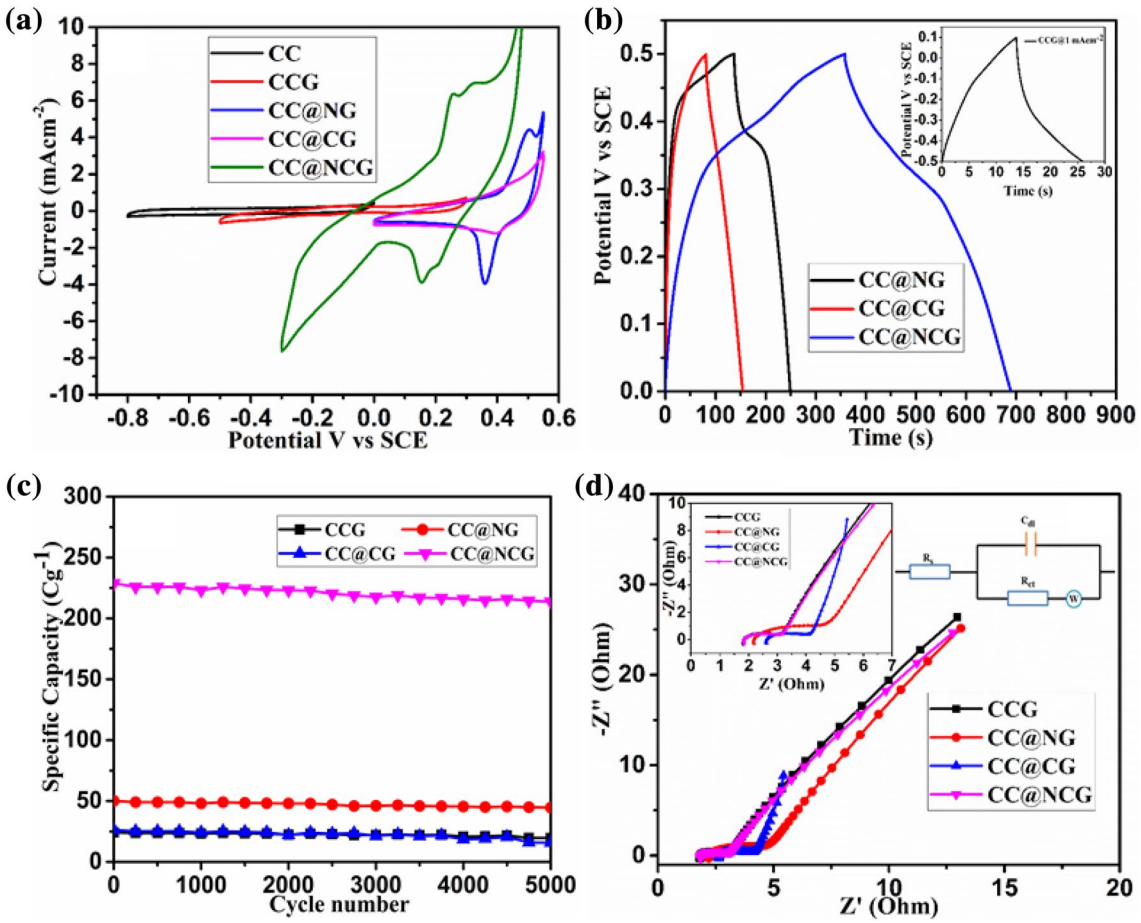

Fig. 6 **a** Cyclic voltammogram of pure and hybrid electrode at 5 mV s^{-1}, **b** charge/discharge curves of hybrid electrodes at 1 mA cm^{-2} (inset for CCG), **c** cyclic stability of the electrodes at 5 mA cm^{-1} (for CCG at 1 mA cm^{-1}), **d** Nyquist plot of pure and hybrid electrode and the inset represents the corresponding extended view (left) and equivalent circuit (right)

$NiCo_2O_4$ nanoparticles and residual oxygen containing functional groups on the rGO as suggested by the wang et al. [50]. In addition the intimate binding with CC affords facile electron transport within the metal oxide and graphene sheets thereby both the redox features were clearly observed. Noticeably, no appropriate redox peaks could be seen in the CV curve of the CC@CG electrode due to the poor conductivity of Co_3O_4. This results were further confirmed with the scan-rate dependent CV analysis as shown in Fig. S3b–d. When the scan rate is increased from 5 to 50 mV s^{-1}, the redox peaks in the CV curve shifted appropriately, which suggest low polarization of the electrodes. From the CV graphs, it can be seen that the peak current increases approximately linear with the square root of the scan rate (not shown here), indicating diffusion controlled faradaic reactions [49]. For further confirmation of the electrochemical activity, constant current charge–discharge analysis was carried out and shown in Fig. 6b. The measured charge–discharge profile at 1 mA cm^{-2} for all the composite electrodes are consistent with the CV results and showed faradaic type energy storage features with quasi nonlinear charge–discharge curves. Since the discharge time is directly controlled by the rate of electrolyte ions diffusion into and out of the electrode surface, the electrochemical activity can be described with their discharge time. The CC@NCG electrode exhibits a much longer discharge time than the pristine and monometallic composite electrodes. This can be ascribed to an increased redox reactions arises by hybrid structure that offer high electrical conductivity and more active sites of the bimetallic electrode. To further quantify the specific capacity, the charge–discharge test was measured at various specific current and displayed in Fig. S4a–d. The similar trends were observed for all the electrodes by varying the specific current from 1 to 10 mA cm^{-2} suggesting that good rate capability of hybrid electrodes. Due to the observed non-capacitive faradaic charge compensation in hybrid electrodes, it does not make sense to calculate the 'specific capacitance' which is not a constant throughout the measured potential regime [47]. Hence, the specific

capacity or the amount of charge stored in the electrode was calculated using, $C_s = It/m$, where I is applied current, t is discharge time and m is the mass of the active material [51, 52]. Thereby, the capacity should be termed in C g^{-1} or mA h g^{-1}, which provides a real metric value of the electrode against other capacitive materials. The specific capacity values of these hybrid composite electrodes are shown in Table 1. Obviously, the estimated specific capacity was found to be high for CC@NCG electrode, is 333.3 C g^{-1} at an applied current of 1 mA cm^{-2} and reduced to 184.7 C g^{-1} at higher current of 10 mA. It has retained its 55.2% of the initial capacity values when the current was increased tentimes, whereas, the estimated specific capacity for pristine and CC@NG and CC@CG composites are 24.2, 124.8, and 61.7 C g^{-1} respectively at 1 mA cm^{-2}. In terms of better vicinity to the readers, the specific capacitance was also calculated simply by dividing the specific capacity value with the corresponding potential (0.8 V for pristine and 0.5 V composites) and the values are tabulated. The bare carbon cloth showed negligible specific capacitance of 3.4 mF g^{-1} from the charge discharge measurement (not shown here). From this value it can be observed that CC@NCG electrode exhibit superior electrochemical performance when compared to their monometallic oxides and the other materials reported earlier. Our specific capacitance are significantly higher than the values reported 221 F g^{-1} at 0.6 A g^{-1} for meso-porous Co_3O_4 [53] and 461 F g^{-1} at 0.2 A g^{-1} for NiO/rGO composites [54]. Also, this value is much higher than 415 F g^{-1} at 3 A g^{-1} in 6 M KOH electrolyte for Co_3O_4/rGO composite prepared via hydrothermal technique [55]. Furthermore, our electrode performance is even better than the value of 508 F g^{-1} at 0.5 A g^{-1} for $NiCoO_2$/rGO composite electrode reported by Liu et al. [56]. The high specific capacity is mainly derived from the highly porous texture with more active sites, and the redox transformation between different states of Ni and Co ions. Noteworthy, the observed specific capacity values are even much higher than the synergistic value of the individual oxides. This can be explained by the presence of rGO in the electrode which significantly enhanced the contribution of both Ni and Co ions for redox process as observed from the CV analysis thereby high specific capacity was obtained. The stability of the electrode is one of the most substantial factors for their practical applications. Hence the electrode was tested by continuous charge–discharge analysis at 5 mA cm^{-2} upto 5000 cycles as shown in Fig. 6c. It demonstrate that the stability of the electrode was quite good for all the electrodes, however the CC@NCG hybrid electrode showed better capacity retention of about 89% after 5000 cycles, whereas the monometallic composites delivered 85 and 81% for CC@CG and CC@NG respectively. It is worth mentioning that pristine CCG electrode showed high capacity retention of 92% indicating the presence of rGO in the CC could increase the cyclic stability of the electrodes. To further interrogate the electrochemical performance, the EIS analysis was performed in the frequency range of 100 kHz to 0.01 Hz at open circuit potential with an AC perturbation of 5 mV. The resultant Nyquist plots are shown in Fig. 6d and the insets showed the enhanced view of high frequency region (left) and the corresponding equivalent circuit (right). The sloped line in the low frequency range corresponds to Warburg impedance (W) followed by the visible semicircle at high frequency regime, shows that diffusion controlled electrochemical capacitive behavior of the composite electrodes. Among them, CC@NCG electrode exhibits small charge transfer resistance as seen in Fig. 5d infers the high electrical conductivity. These results can be due to the hybrid structure of graphene and $NiCo_2O_4$ nanoparticle integrated onto porous carbon cloth which could promote the rapid electron and electrolyte transportation at the electrode surface [30].

The electro-catalytic activity of metal oxide/rGO hierarchical architecture on CFC towards methanol oxidation was evaluated within the alkaline medium. Since the bare carbon cloth and pristine CCG showed poor methanol oxidation only metal oxide/rGO composites are further studied for methanol oxidation. Figure 7a represents the CV curves of MO/rGO@CC catalysts under 1 M KOH at a sweep rate of 2 mV s^{-1}. Without the methanol, CV curve shows the visible pair of redox peak over the measured potential range which demonstrates the surface redox process [10, 57] and the sharp increase in anodic current in the CV curve

Table 1 Electrochemical charge storage capability of the electrodes

Electrode materials	Specific capacity from charge–discharge studies in C g^{-1}			Specific capacitance from charge–discharge studies in F g^{-1}		
	1 mA	5 mA	10 mA	1 mA	5 mA	10 mA
CC	–	–	–	3.4 (mF g^{-1})	–	–
CCG	24	–	–	30.25	–	–
CC@NG	124.8	50	25.1	249.6	100	50.2
CC@CG	61.7	26.2	17.5	123.4	52.4	35
CC@NCG	333.3	228.4	184.7	666.6	456.8	369.4

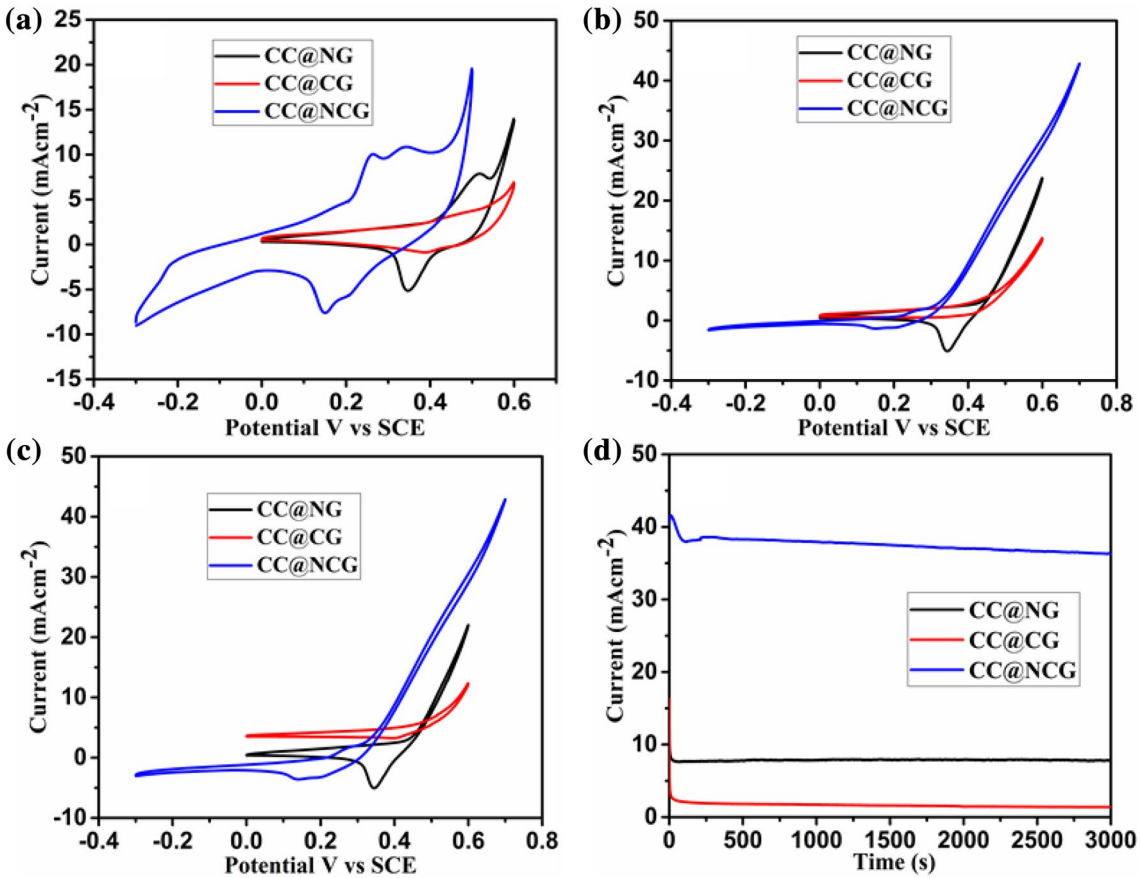

Fig. 7 **a** Cyclic voltammogram of hybrid electrode measured in 1 M KOH, **b** 1 M KOH + 0.5 M CH_3OH at 5 mV s^{-1}. **c** CV curves of the hybrid electrodes after 500 cycles at 20 mV s^{-1}. **d** Amperometric curves of the hybrid electrodes at 0.4 V

measured with 0.5 M CH_3OH reveals the methanol oxidation of the catalyst as shown in Fig. 7b. The mechanism for electro-oxidation of methanol by this CC@NCG composite electrode is as follows (Eqs. 5–7) which is the combination of individual oxides as reported earlier [58].

$$NiCo_2O_4 + OH^- + H_2O \leftrightarrow NiOOH + 2CoOOH + e^- \quad (5)$$

$$NiOOH + CH_3OH + xO_2 \rightarrow Ni(OH)_2 + CO_2 + yH_2O \quad (6)$$

$$2CoOOH + mCH_3OH + nO_2 \leftrightarrow 2Co(OH)_2 + 2CO_2 + zH_2O \quad (7)$$

Noticeably, an increase in the anodic peak current and decrease of cathodic peak current during the negative sweep was observed in the CV curve with the presence of methanol. The methanol oxidation current for CC@NCG is much higher at 0.7 V and exhibits a lower onset potential (~0.3 V) as well. The monometallic oxide composites shows higher onset potential of 0.43 and 0.45 V for CC@NG and CC@CG respectively. Interestingly, the low onset potential for CC@NCG electro-catalyst was observed when compared to monometallic oxides and as reported earlier (~0.4 V) [59] indicates that there is a scope for nanostructured metal oxide/rGO composite electro-catalyst for DMFCs. The maximum current density of 43 mA cm^{-2} was observed and which is comparatively higher than the earlier report [32, 59]. These result evidences the superior electro-catalytic performance of the hybrid $NiCo_2O_4$/rGO nanostructure. Further the methanol reacts with the proposed catalyst components as suggested reactions, initially MOOH (M = Ni and Co) formed on the electrode surface and increases the anodic current and decreases the corresponding reverse cathodic current. The scan rate dependent electro-catalytic activity of composite electro-catalysts was investigated using CV under 0.5 M CH_3OH. Figure S5a–c indicates the CV curves measured at different scan rate ranging from 5 to 50 mV s^{-1}. It reveals that the hybrid nanostructure showed the increasing oxidation current with the scan rate and describes the rapid ion/electron transfer within the electrode. At a high scan rate of 50 mV s^{-1} high anodic current was observed and it retained even at a low scan rate of 5 mV s^{-1} which ascribes the greater electro-catalytic activity of the hybrid electrodes. The catalytic stability of these metal oxide/rGO hybrid catalysts towards methanol oxidation were investigated by repeated cyclic voltammogram at a 20 mV s^{-1}

over 500 cycles and shown in Fig. 7c. It can be seen that the catalytic activity of the electrode even after 500 cycles was excellent and demonstrates the good stability. Further, chronoamperometic curve at 0.4 V for an extended time of 3000 s is shown in Fig. 7d. The initial loss upto 50 s followed by stable curve noticed upto 2950s indicates the long term stability of this hybrid nanostructure. The slight fluctuation in the amperometric for CC@NCG curve indicates the influence of generated gases during methanol oxidation [60]. The excellent methanol oxidation behavior of these hybrid catalysts was further evaluated with the electrochemical impedance spectra (EIS) measurement. Figure S5d shows the EIS spectra of hybrid electro-catalysts with methanol. The observed Nyquist plot consists of visible semicircle at high frequency region and extended tail at low frequency region related to the charge transfer resistance and pseudocapacitance over the metal oxide surface respectively. From the EIS spectra it can be observed that the R_{ct} value has been increased slightly during methanol oxidation process due to methanol adsorption. It was noticeable that the diameter of the semicircle is small and can be understandable from the superior electrical conductivity of the catalyst in 0.5 M CH_3OH. The observed impedance spectra were compared to the equivalent circuit as given in the inset of Fig. 6d. According to the equivalent circuit, R_s, C_{dl}, R_{ct}, and W are the solution resistance, double layer capacitance, charge transfer resistance and Warberg's diffusion elements, respectively [60]. With 0.5 M CH_3OH, the estimated solution resistance values were ~2.2, 2.6 and 4.5 Ω for CC@NG, CC@CG and CC@NCG respectively. This indicates that our hybrid nanostructures on CC substrate exhibit the good tolerance against the methanol adsorption or intermediates oxidation. Furthermore, the effective contribution of both $Ni^{2+/3+}$ and $Co^{2+/3+}$ for methanol oxidation process and thereby enhanced solution resistance of CC@NCG hybrid electrode is clearly confirmed. The excellent electrical conductivity, and admirable mechanical integrity between CC and metal oxide/rGO facilitates rapid electron transfer within the electrode which results in high catalytic current density. Therefore it can be concluded that, since during the methanol oxidation, the CC@NCG catalyst retained their high electrical conductivity with negligible CO poisoning and has long-term stability, therefore, the developed composite material would serve as a promising electro-catalyst in DMFCs.

The bi-functional electrochemical activity with high charge storage capacity, high rate and cycling capability, and excellent electro oxidation of methanol with high current density demonstrates the high performance characteristics of these hybrid electrode materials. This can be explained by the following structural features of the electrode. Firstly, the incorporation of rGO offers coarse morphology with lot of pores and leads to the fast electron/ion transfer within the electrode. The addition of rGO further enhance the electronic conductivity of the electrode thus enhance the specific capacity for the hybrid electrodes. Finally, the stable bonding between CFC and metal oxide provide good mechanical integrity for the electrode which increase the electrochemical stability of the electrode for long term applications. However, the exact reason for the superior performance is not clear and need further investigations related to microstructure and composition which are in progress.

5 Conclusions

A reduced graphene oxide supported NiO, Co_3O_4 and $NiCo_2O_4$ electrode-catalysts were synthesized via facile one step hydrothermal technique. The hybrid electrodes have been demonstrated for both non-capacitive energy storage and electro-oxidation of methanol in alkaline solution. Because of good conductivity and intimate contact with CC support, the CC@NCG composite electrode exhibited superior specific capacity of 333.3 C g^{-1} with excellent cyclic stability. In addition, the proposed hybrid materials exhibit greater electro-catalytic activity toward methanol oxidation and excellent tolerance against intermediates with long term stability. The above superior electrochemical performances for CC@NCG electrode when compared to their monometallic ones were due to the more active sites from synergistic contribution of both Ni and Co ions, mechanical stability and good conductivity of CC support. The present study validates that reduced graphene oxide reinforced metal oxide hybrid with dual-functionality would be an encouraging substitute of expensive electrode or catalyst systems for high performance energy storage and conversion devices applications.

References

1. M. Winter, R.J. Brodd, What are batteries, fuel cells, and supercapacitors? Chem. Rev. **104**, 4245–4269 (2004)
2. P. Simon, Y. Gogotsi, Materials for electrochemical capacitors. Nat. Mater. **7**, 845–854 (2008)
3. J.R. Miller, P. Simon, Electrochemcial capacitors for energy management. Science **321**, 651–652 (2008)
4. M. Osiak, H. Geaney, E. Armstrong, C. O'Dwyer, Structuring materials for lithium ion batteries: advancements in nanomaterial structure, composition, and defined assembly on cell performance. J. Mater. Chem. A **2**, 9433–9460 (2014)
5. H.B. Li, M.H. Yu, F.X. Wang, P. Liu, Y. Liang, J. Xiao, C.X. Wang, Y.X. Tong, W. Yang, Amorphous nickel hydroxide nanospheres with ultrahigh capacitance and energy density as electrochemical pseudocapacitor materials. Nat. Commun. **4**, 18904 (2013)
6. T. Brezesinski, J. Wang, S.H. Tolbert, B. Dunn, Ordered mesoporous alpha-MoO_3 with iso-oriented nanocrystalline walls for thin film supercapacitors. Nat. Mater. **9**, 146–151 (2009)

7. M. Toupin, T. Brousse, D. Belanger, Charge storage mechanism of MnO_2 electrode used in aqueous electrochemical capacitor. Chem. Mater. **16**, 3184–3190 (2004)
8. J.W. Long, B. Dunn, D.R. Rolison, H.S. White, Three-dimensional battery architecture. Chem. Rev. **104**, 4463–4492 (2004)
9. J. Wang, J. Polleux, J. Lim, B. Dunn, Pseudocapcitive contributions to electrochemical energy storage in TiO_2 (anatase) nanoparticles. J. Phys. Chem. C **111**, 14925–14931 (2007)
10. Y. Xiang, S. Lu, P. Jiang, Layer-by-layer self-assembly in the development of electrochemical energy conversion and storage devices from fuel cells to supercapacitors. Chem. Soc. Rev. **41**, 7291–7321 (2012)
11. C. Zhifan, Z. Hongbin, Z. Jiujun, X. Jiaqiang, IrNi nanoparticle-decorated flower-shaped $NiCo_2O_4$ nanostructures: controllable synthesis and enhanced electrochemical activity for oxygen evolution reaction. Sci. China. Mater. **60**(2), 119–130 (2017)
12. S. Cheng, L. Yang, Y. Liu, W. Lin, L. Huang, D. Chen, C.P. Wong, M. Liu, Carbon fiber paper supported hybrid nanonet/nanoflower nickel oxide electrodes for high performance pseudocapacitors. J. Mater. Chem. A **1**, 7709–7716 (2013)
13. Z. Jingwen, C. Jiale, X. Simin, S. Mingfei, Y. Dongpeng, W. Min, G.E. David, D. Xue, CoMn-layered double hydroxide nanowalls supported on carbon fibers for high-performance flexible energy storage devices. J. Mater. Chem. A **1**, 8836–8843 (2013)
14. Y. Zeheng, X. Feifei, Z. Weixin, M. Zhousheng, P. Bo, Z. Xiao, Controllable preparation of multishelled NiO hollow nanospheres via layer-by-layer self-assembly for supercapacitor application. J. Power Sources **246**, 24–31 (2014)
15. T. Jun, L. Dequan, Z. Yunxian, L. Xiuwan, W. Xinghui, H. Deyan, Effect of Zn-substitution on cycling performance of α-$Co(OH)_2$ nanosheet electrode for supercapacitors. J. Mater. Chem. A. **2**, 2585–2591 (2014)
16. Y.C. Chen, Y.K. Hsub, Y.G. Lina, Y.K. Lin, Y.Y. Horng, L.C. Chen, K.H. Chen, Highly flexible supercapacitors with manganese oxide nanosheet/carbon cloth electrode. Electrochim. Acta **56**, 7124–7130 (2011)
17. C. Shuang, Z. Teng, L. Xi-Hong, Z. Man-Zhi, L. Zhuo-Ying, X. Chang-Wei, T. Yexiang, Large-area manganese oxide nanorod arrays as efficient electrocatalyst for oxygen evolution reaction. Int. J. Hydr. Energy **37**, 13350–13354 (2012)
18. D. Rui, Q. Li, J. Mingjun, W. Hongyu, Porous $NiCo_2O_4$ nanostructures as bi-functional electrocatalysts for CH_3OH oxidation reaction and H_2O_2 reduction reaction. Electrochim. Acta **113**, 290–301 (2013)
19. Y. Mengqi, W. Sunli, H. Jiayi, C. Zheyan, B. Yihui, W. Lanju, C. Jianrong, W. Xuexiang, Additive-free macroscopic-scales synthesis of coral-like nickel cobalt oxides with hierarchical pores and their electrocatalytic properties for methanol oxidation. Electrochim. Acta **145**, 300–306 (2014)
20. D. Rui, Q. Li, J. Mingjun, W. Hongyu, Sodium dodecyl sulfate-assisted hydrothermal synthesis of mesoporous nickel cobaltite nanoparticles with enhanced catalytic activity for methanol electrooxidation. J. Power Sources **251**, 287–295 (2014)
21. W. Yonggang, S. Yanfang, X. Yongyao, Electrochemical capacitors: mechanism, materials, systems, characterization and applications. Chem. Soc. Rev. **45**, 5925–5950 (2016)
22. Z. Qifeng, U. Evan, L.C. Stephanie, C. Guozhong, Nanomaterials for energy conversion and storage. Chem. Soc. Rev. **42**, 3127–3171 (2013)
23. R. Yu, M. Zhen, G.B. Peter, Ordered mesoporous metal oxides: synthesis and applications. Chem. Soc. Rev. **41**, 4909–4927 (2012)
24. W. Guoping, Z. Lei, Z. Jiujun, A review of electrode materials for electrochemical supercapacitors. Chem. Soc. Rev. **41**, 797–828 (2012)
25. L. Huang, D. Chen, Y. Ding, S. Feng, Z.L. Wang, M. Liu, Nickel-cobalt hydroxide nanosheets coated on $NiCo_2O_4$ nanowires grown on carbon fiber paper for high performance pseudocapacitors. Nano Lett. **13**, 3135–3139 (2013)
26. W. Hailiang, S.C. Hernan, L. Yongye, D. Hongjie, $Ni(OH)_2$ nanoplates grown on graphene as advanced electrochemical pseudocapacitor materials. J. Am. Chem. Soc. **132**, 7472–7477 (2010)
27. L. Lili, N. Zhiqiang, C. Jun, Unconventional supercapacitors from nanocarbon-based electrode materials to device configurations. Chem. Soc. Rev. **45**, 4340–4363 (2016)
28. L. Bin, Z. Jun, W. Xianfu, C. Gui, C. Di, Z. Chongwu, S. Guozhen, Hierarchical three-dimensional $ZnCo_2O_4$ nanowire arrays/carbon cloth anodes for a novel class of high-performance flexible lithium-ion batteries. Nano Lett. **12**, 3005–3011 (2012)
29. Y. Wanlu, G. Zan, M. Jing, Z. Xingming, W. Jun, L. Jingyuan, Hierarchical $NiCo_2O_4$@NiO core–shell heterostructured nanowire arrays on carbon cloth for a high-performance flexible all-solid-state electrochemical capacitor. J. Mater. Chem. A **2**, 1448–1457 (2014)
30. N. Padmanathan, S. Selladurai, Controlled growth of spinel $NiCo_2O_4$ nanostructures on carbon cloth as a superior electrode for supercapacitors. RSC Adv. **4**, 8341–8349 (2014)
31. W. Huanwen, W. Xuefeng, Growing nickel cobaltite nanowires and nanosheets on carbon cloth with different pseudocapacitive performance. ACS Appl. Mater. Interfaces **5**, 6255–6260 (2013)
32. N. Padmanathan, S. Han, S. Selladurai, G. Colm, C. O'Dwyer., M.R. Kafil, Pseudocapacitance of α-$CoMoO_4$ nanoflakes in non-aqueous electrolyte and its bi-functional electro catalytic activity for methanol oxidation. Int. J. Hydr. Energy **40**, 16297–16305 (2015)
33. C. Hyun-Jung, J. Sun-Min, S. Jeong-Min, W.C. Dong, D. Liming, B. Jong-Beom, Graphene for energy conversion and storage in fuel cells and supercapacitors. Nano Energy **1**, 534–551 (2012)
34. D. Xiao-Chen, X. Hang, W. Xue-Wan, H. Yin-Xi, B.C.P. Mary, Z. Hua, W. Lian-Hui, H. Wei, C. Peng, 3D graphene cobalt oxide electrode for high-performance supercapacitor and enzyme less glucose detection. ACS Nano **6**, 3206–3213 (2012)
35. B. Yang, L. Miaomiao, S. Jing, G. Lian, Fabrication of Ni–Co binary oxide/reduced graphene oxide composite with high capacitance and cyclicity as efficient electrode for supercapacitors. Ionics **22**, 535–544 (2016)
36. G. Feng, W. Qing, Y. Jiaxiang, B. Hong, W. Mingtai, Synthesis of graphene/nickel oxide composite with improved electrochemical performance in capacitors. Ionics **19**, 1883–1889 (2013)
37. Y. Mei, C. Jianpeng, L. Jianhua, L. Songmei, M. Yuxiao, Z. Jingdan, A. Junwei, Mesoporous $NiCo_2O_4$ nanoneedles grown on 3D graphene-nickel foam for supercapacitor and methanol electrooxidation. Electrochim. Acta **151**, 99–108 (2015)
38. D.K. Hassen, M.M. Selim, S.A. El-Safty, K.A. Khalil, G. Abu el-Maged, M. Dewidar, Graphene-supported $Co(OH)_2$ mesostructures for ethanol oxidation reaction electrocatalysis. Nano Struct. Nano Objects **9**, 31–39 (2017)
39. L. Su-Juan, X. Ning, L. Xia-Lei, Z. Meng-Meng, Y. Bai-Qing, P. Huan, A facile one-step electrochemical synthesis of graphene/NiO nanocomposites as efficient electrocatalyst for glucose and methanol. Sens. Actuators B **190**, 809–817 (2017)
40. L. Qian, W. Qiang, X. Lijing, C. Chengmeng, L. Chunxiang, S. Fang-Yuan, Z. Pucha, Layered NiO/reduced graphene oxide composites by heterogeneous assembly with enhanced performance as high-performance asymmetric supercapacitor cathode. RSC Adv. **6**, 46548–46557 (2016)
41. J. Lavanya, N. Gomathi, S. Neogi, Electrochemical performance of nitrogen and oxygen radio-frequency plasma induced functional groups on tri-layered reduced graphene oxide. Mater. Res. Express **1**, 025604 (2014)

42. Z. Tingting, H. Chuansheng, S. Fengzhan, D. Yongqi, W. Manchao, P. Lin, W. Jiahui, L. Yuqing, Co_3O_4 nanoparticles anchored on nitrogen-doped reduced graphene oxide as a multifunctional catalyst for H_2O_2 reduction, oxygen reduction and evolution reaction. Sci. Rep. **7**, 43638 (2017)
43. L. Wei, X. Lipeng, X. Xin, L. Qida, Z. Ming, D. Shujiang, Z. Mingshu, L. Xiaojie, Facile synthesis of three-dimensional structured carbon fiber-$NiCo_2O_4$-$Ni(OH)_2$ high-performance electrode for pseudocapacitors. Sci. Rep. **5**, 9277 (2015)
44. H. Jianlin, W. Junying, W. Congwei, Z. Huinian, C. Lu, J. Wang, Hierarchical porous graphene carbon-based supercapacitors. Chem. Mater. **27**, 2107–2113 (2015)
45. D. Chen, Q. Wang, R. Wang, G. Shen, Ternary oxide nanostructured materials for supercapacitors: a review. J. Mater. Chem. A **3**, 10158–10173 (2015)
46. J. Hoon Chae, X. Zhou, G. Zheng Chen, From electrochemical capacitors to supercapatteries. Green **2**, 41–54 (2012)
47. T. Brousse, D. B´elanger, J.W. Long, To be or not to be pseudocapacitive? J. Electrochem. Soc. **62**(5), A5185–A5189 (2015)
48. S.W. Zhang, G.Z. Chen, Manganese oxide based materials for supercapacitors. Energy Mater. **3**, 186–200 (2008)
49. S. Gao, F. Liao, S. Ma, L. Zhu, M. Shao, Network-like mesoporous $NiCo_2O_4$ grown on carbon cloth for high-performance pseudocapacitors. J. Mater. Chem. A **3**, 16520–16527 (2015)
50. H.W. Wang, Z. Hu, Y. Chang, Y. Li Chen, H.Y. Wu, Z.Y. Zhang, Y.Y. Yang, Design and synthesis of $NiCo_2O_4$-reduced graphene oxide composites for high performance supercapacitors. J. Mater. Chem. **21**, 10504–10511 (2011)
51. J. Ding, H. Wang, Z. Li, K. Cui, D. Karpuzov, X. Tan, A. Kohandehghan, D. Mitlin, Peanut shell hybrid sodium ion capacitor with extreme energy–power rivals lithium ion capacitors. Energy Environ. Sci. **8**, 941–955 (2015)
52. N. Padmanathan, H. Shao, D. McNulty, C. O'Dwyer, K.M. Razeeb, Hierarchical NiO–In_2O_3 microflower (3D)/nanorod (1D) hetero-architecture as a supercapattery electrode with excellent cyclic stability. J. Mater. Chem. A **4**, 4820–4830 (2016)
53. A. Jena, N. Munichandraiah, S.A. Shivashankar, Morphology controlled growth of Meso-porous Co3O4 nanostructures and study of their electrochemical capacitive behavior. J. Electrochem. Soc. **159**, A1682–A1689 (2012)
54. Y. Bu, S. Wang, H. Jin, W. Zhang, J. Lin, J. Wang, Synthesis of porous NiO/reduced graphene oxide composites for supercapacitors. J. Electrochem. Soc. **159**, A990–A994 (2012)
55. C. Yuan, L. Yang, L. Hou, J. Li, Y. Sun, X. Zhang, L. Shen, X. Lu, S. Xiong, X.W. Lou, Flexible hybrid paper made of monolayer Co_3O_4 microsphere arrays on rGO/CNTs and their application in electrochemical capacitors. Adv. Funct. Mater. **22**, 2560–2566 (2012)
56. Y. Xu, J. Wei, L. Tan, J. Yu, Y. Chen, A facile approach to $NiCoO_2$ intimately standing on nitrogen doped graphene sheets by one-step hydrothermal synthesis for supercapacitors. J. Mater. Chem. A **3**, 7121–7131 (2015)
57. R.N. Singh, T. Sharma, A. Singh, Anindita, D. Mishra, Electrocatalytic activities of nano-sized spinel-type $Cu_xCo_{3-x}O_4$ ($0 \leq x \leq 1$) for methanol oxidation in alkaline solutions. Int. J. Electrochem. Sci. **2**, 762–777 (2007)
58. T.H. Ko, K. Devarayan, M.K. Seo, H.Y. Kim, B.S. Kim, Facile synthesis of core/shell like $NiCo_2O_4$-decorated MWCNTs and its excellent electrocatalytic activity for methanol oxidation. Sci. Rep. **6**, 20313 (2016)
59. D. Ashok Kumar, R.K. Layek, N.H. Kim, D.J. Joong Hee Lee, Reduced graphene oxide (RGO)-supported $NiCo_2O_4$ nanoparticles: an electrocatalyst for methanol oxidation. Nanoscale **6**, 10657–10665 (2014)
60. R. Ding, L. Qi, M. Jia, H. Wang, Facile synthesis of mesoporous spinel $NiCo_2O_4$ nanostructures as highly efficient electrocatalysts for urea electro-oxidation. Nanoscale **6**, 1369–1376 (2014)